



HAL
open science

A Novel Optical Wireless Modulation exploiting Time, Frequency and Amplitude divisions enabling Link and Illumination Reliability

Andrea Petroni, Antonio Costanzo, Valeria Loscrì, Mauro Biagi

► To cite this version:

Andrea Petroni, Antonio Costanzo, Valeria Loscrì, Mauro Biagi. A Novel Optical Wireless Modulation exploiting Time, Frequency and Amplitude divisions enabling Link and Illumination Reliability. IEEE Transactions on Wireless Communications, 2023, 10.1109/TWC.2023.3285822 . hal-04115865

HAL Id: hal-04115865

<https://hal.science/hal-04115865>

Submitted on 2 Jun 2023

HAL is a multi-disciplinary open access archive for the deposit and dissemination of scientific research documents, whether they are published or not. The documents may come from teaching and research institutions in France or abroad, or from public or private research centers.

L'archive ouverte pluridisciplinaire **HAL**, est destinée au dépôt et à la diffusion de documents scientifiques de niveau recherche, publiés ou non, émanant des établissements d'enseignement et de recherche français ou étrangers, des laboratoires publics ou privés.



Distributed under a Creative Commons Attribution 4.0 International License

A Novel Optical Wireless Modulation exploiting Time, Frequency and Amplitude divisions enabling Link and Illumination Reliability

Andrea Petroni, Antonio Costanzo, *Member, IEEE*

Valeria Loscri, *Senior Member, IEEE*, and Mauro Biagi, *Senior Member, IEEE*

Abstract

The simultaneous task of data transmission and illumination achievable with Visible Light Communication is continuing to raise the interest of research and industry community. The joint use of the same infrastructure for illumination and communication may enable new location-based services, by implementing sensing functionalities. In this paper, we propose a new multi-dimensional modulation scheme combining different techniques, in order to increase the spectral and energy efficiency, while meeting the optical power emission constraints. Specifically, Pulse Position Modulation Pulse Amplitude Modulation and Frequency Shift Keying are effectively combined in a joint fashion, in order to exploit time, amplitude and frequency information. The innovation of using a smart combination of those modulation formats is based on the exploitation of specific features of the different approaches. In particular, we combine time, amplitude and frequency features to enhance the robustness of the system, without sacrificing the data rate performance as for coded systems. The major implication of such approach is twofold. In this way, we grant a constant illumination level per symbol and, moreover, we outperform in terms of reliability coded modulations for the same level of spectral efficiency. Theoretical results, validated through experimental evaluations, demonstrate that the combined approach achieves very good performance.

Andrea Petroni is with Fondazione Ugo Bordoni (FUB), Viale America, 201 00144 Rome, Italy (e-mail: apetroni@fub.it).

Mauro Biagi is with the Department of Information, Electrical, and Telecommunication (DIET) engineering, “Sapienza” University of Rome, Via Eudossiana, 18 00184 Rome, Italy (e-mail: mauro.biagi@uniroma1.it).

Antonio Costanzo is with LEOST Team at Université Gustave Eiffel, France (e-mail: antonio.costanzo@univ-eiffel.fr).

Valeria Loscri is with FUN Team of Inria Lille, France (e-mail: valeria.loscri@inria.fr).

Index Terms

Modulation, Coding, Illumination, Detection, Optical Wireless

I. INTRODUCTION

It is a well recognized matter of fact that the Internet of Everything (IoE) paradigm main limitation is represented by the exiguous wireless resources [1]. In the last decade, Optical Wireless Communication Systems (OWCSs) have risen as a green and effective solution to alleviate the spectral scarcity and boost the ubiquitous deployment and usage of IoE devices [2]. The significant advances in optoelectronic technology have made Light Emitting Diodes (LEDs) and photodetectors (PDs) inexpensive, and efficient hardware to equip optical transceivers [3]. Furthermore, the emission of LEDs can be conveniently managed to provide the illumination service jointly with wireless connectivity. Such scenario is peculiar of the so called Visible Light Communication (VLC) [4], representing one of the most promising fields of application for OWCSs.

By focusing on communication aspects, the design of energy efficient and effective modulation schemes is paramount to maximize the performance in terms of both data rate and reliability [5]. One of the key features of OWCSs is they are Intensity-Modulation/Direct-Detection (IM/DD) systems, requiring high energy efficient modulation techniques. Among the different modulation schemes, one of the most widespread is On-Off Keying (OOK), as a special case of Pulse-Amplitude Modulation (PAM) employing only two transmit signal power levels, one of which is set to zero. In general, even though PAM is very suitable for OWCSs, its main issue is related to the growth of the electrical/optical energy per bit, with the increase of modulation order, necessary to guarantee a certain Bit Error Rate (BER). A higher level of energy efficiency can be achieved with the adoption of orthogonal modulation schemes, although with a negative impact on spectral efficiency. Frequency-Shift Keying (FSK) belongs to the orthogonal modulation schemes category [6]. Its main drawback in the context of OWCSs is represented by its bipolar characteristics, however the variant of FSK based on Direct-Current (DC) offset, namely DC-FSK, allows to obtain a scheme compatible with the IM/DD approach [7]. In fact, from an energy point of view, DC-FSK is more efficient than an asymmetric version of FSK, but suffers from a greater spectral efficiency reduction. Another orthogonal modulation technique is represented by Pulse

46 Position Modulation (PPM) [8]. PPM is interesting for OWCSs since particularly fitting also for
47 localization purposes, but its inefficiency concerns the peak-to-mean optical power ratio [9].

48 Based on these premises, it is clear that each modulation scheme has its own strengths and
49 weaknesses. Hence, combining different techniques would be a promising approach to capitalize
50 on the benefits and mitigate drawbacks. One of the earliest proposal for hybrid schemes is
51 described in [10], where a low-density parity-check coded hybrid subcarrier-amplitude-phase-
52 polarization modulation is investigated to deal with optical channels and providing up to 240-
53 Gb/s rate. Another work about hybrid solutions for OWCSs has been presented in [11]. The
54 authors propose a class of optical modulation techniques as a combination of PPM and FSK
55 and with the addition of a polarization component and/or phase modulation, demonstrating the
56 achievement of a higher power efficiency. Both the schemes in [10], [11] were developed for
57 optical systems, but not specifically wireless, hence potential issues related to dimming control,
58 typical of indoor VLC, are not addressed. A hybrid DC Frequency and Phase Shift Keying
59 modulation scheme for optical wireless systems has been investigated in [12]. The authors
60 established the particular combination of phase and frequency leading to an optimal energy
61 and spectral efficiency. Phase and frequency shift applied to OOK are considered by the authors
62 in [13] to demonstrate the feasibility of a 160 meters outdoor VLC link, by employing an image
63 sensor-based receiver for reliable signal detection. Still dealing with free space optics (FSO), the
64 joint use of quadrature amplitude modulation and multi-pulse position modulation is evaluated
65 in [14] for both turbulence-free and gamma-gamma channels, with results demonstrating its
66 superiority to other known schemes in terms of power efficiency and outage probability. Although
67 the techniques in [12]–[14] are tailored to optical wireless communications, no focus has been
68 made on their application in indoor VLC systems, therefore performance related to lighting
69 control were not investigated. An interesting contribution on hybrid modulation schemes has been
70 proposed in [15], where the authors combine Pulse Width Modulation, PPM and Discrete Pulse
71 Amplitude Modulation (DPAM) in order to increase the data transmission rate. Furthermore, the
72 use of DPAM is also aimed to achieve the dimming function. Similarly, the features of DPAM
73 and the reliability of variable PPM are jointly exploited in [16] to improve the communication
74 rate while providing illumination control as well. The effectiveness of the approaches presented
75 in [15] and [16] was validated through several experiments, however the lack of preliminary
76 simulation analysis does not allow the measured performance to be compared with a reliable
77 benchmark. Besides in [17] a new modulation format able to constrain macro-symbol by macro-

78 symbol the lighting level has been proposed by merging PAM and PPM. The receiver is really
79 complex and a sub-optimal solution has been proposed in [18].

80 Based on the encouraging results available in the literature, the idea of this work is to
81 explore the potentialities of three popular modulation formats and try to merge them in a whole
82 framework. Hence, in this work we propose a joint multi-modulation scheme, based on the
83 combination of non-orthogonal PPM, PAM and FSK, in order to efficiently exploit the time,
84 amplitude and frequency features of the different schemes.

85 More in detail, it is known from theory [19] that the adoption of spectrally efficient *pure*
86 modulations like PAM allows the achievement of high data rates. However, the main drawback
87 concerns the power inefficiency that, in OWCSs, does not guarantee the provision of a constant
88 lighting level per symbol and, moreover, modulation only is not sufficient to achieve high
89 reliability in real systems. Nonetheless, solving the reliability problem through coding does
90 not allow to solve illumination issues. On the other hand, light emission and robustness to errors
91 can be effectively addressed by using different schemes, such as FSK or PPM, but rate is
92 unavoidably penalized due to the bandwidth inefficiency.

93 With the aim to achieve a convenient compromise between rate and reliability, the use of
94 hybrid modulations has been recently spreading. Current works in the literature mainly deal
95 with the merging of pairs of modulation schemes, typically phase and amplitude, frequency and
96 amplitude, phase and frequency domains. Furthermore, the largest part of the proposed solutions
97 are developed for FSO applications or, in general, not specifically for indoor wireless scenarios.
98 Hence, issues related to power and illumination control that characterize indoor VLC are still
99 very often neglected.

100 The main novelty of this work is that we propose a multi-modulation scheme relying on the
101 combination of non-orthogonal PPM, PAM and FSK to leverage the specific features and smartly
102 mitigate the main drawbacks of each modulation. Such popular schemes are merged in a whole,
103 novel framework, in order to efficiently exploit the time, amplitude and frequency features of
104 the different schemes. The goal is to achieve performance improvements in terms of spectral
105 and power efficiency with respect to pure modulations, providing also a constant illumination
106 level that represents a fundamental requirement in real-world indoor VLC systems. The main
107 contributions can be summarized as follows. The multi-dimensional modulation we propose:

- 108 • is able to simultaneously *exploit* the spectral efficiency of PAM and the power efficiency of
109 PPM and FSK by combining them in a single and more effective scheme, where the impact

of pure modulations weaknesses is reduced;

- is able to grant a constant power level, thus meaning constant lighting level on a per symbol basis, allowing illumination control while other coded and uncoded schemes generally do not;
- allows the use of different receivers, ranging from the optimum to several sub-optimal ones, with each one providing a particular trade off between computational complexity and performance;
- is able to outperform block coding strategies, for the same level of spectral efficiency, in terms of communication reliability, as confirmed by experimental validation as well.

The paper is organized as follows. In Sec.II, we introduce the system model, including channel description and the multi-dimensional modulation we propose. In Sec III, we detail the optimum receiver structure and discuss the implementation of several sub-optimal and less costly receivers. In order to evaluate both the performance of the modulation itself and the different receivers effectiveness, we proceed in Sec. IV with the numerical results description and we also show some test results. Last, in Sec. V we draw final conclusion.

II. SYSTEM MODEL AND PROPOSED MODULATION

Let us consider a point-to-point optical link with transmitter and receiver equipped with a single LED and PD, respectively. The signal propagation can be modeled as:

$$y(t) = \rho h x(t) + w(t) \quad (1)$$

where $x(t)$ is the instantaneous power associated to the transmitted optical signal, h accounts for the channel effect from the source to the receiver, ρ is the responsivity of the PD (measured in ampere/watt), and $y(t)$ is the received current signal resulting from opto-electrical conversion. Finally, $w(t)$ is the noise term modeled as zero-mean, additive white and Gaussian, the variance of which is indicated as σ_w^2 . Regarding the channel characterization, by assuming the signal propagation as Lambertian and line-of-sight, we can model h as [20]:

$$h = \begin{cases} \frac{(n+1)A_{\text{pd}}}{2\pi D^2} \cos^n(\phi) \cos(\psi) g(\psi), & \psi \leq \Psi \\ 0, & \psi > \Psi \end{cases} \quad (2)$$

where A_{pd} is area of the PD, D is the distance between LED and PD, g represents the gain of a potentially employable optical concentrator and $n = -\ln 2 / \ln(\cos \Phi_{1/2})$ represents the

136 Lambertian emission factor derived from the LED -3dB semi-angle. Finally, ϕ and ψ are the
 137 angle of radiance and incidence, respectively, with Ψ defining the PD FOV.

138 Herein, we propose a novel multi-dimensional modulation scheme based on a PPM-like signal-
 139 ing, FSK-inspired shape and also PAM-based modulation. The general framework description
 140 is provided in Figure 1. Transmit side operations are described in the current section, while
 141 received signal processing is detailed in the next one.

142 Now, we proceed by first introducing the generic symbol emitted by the modulator in the
 143 following compact form:

$$x(t) = I_0 + A_m s_n(t - \ell T_c) \quad (3)$$

where I_0 is a light bias that is used to maintain constant the lighting level per symbol. This choice is fundamental in order to guarantee a constant illumination level. In fact, the use of

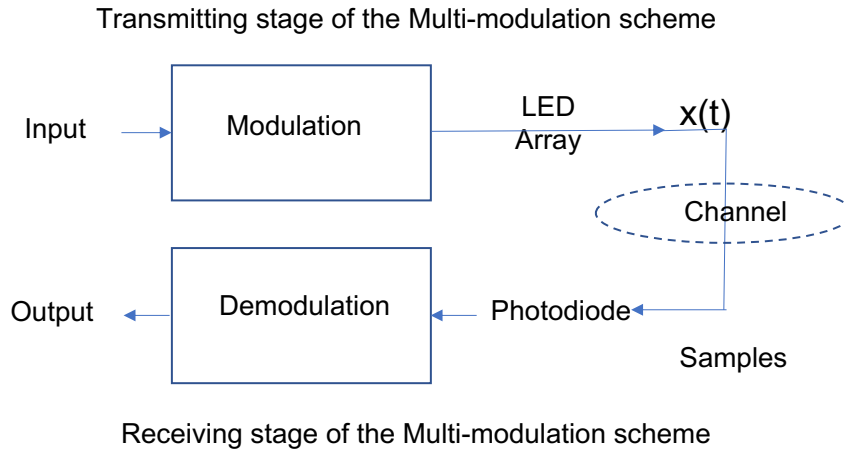


Fig. 1. General framework describing the proposed scheme principles.

different amplitudes, as realized in PAM modulation, allows to have a constant *average* lighting, only under the hypothesis of equal distribution of the transmitted symbols. Unfortunately, such assumption *fails to be verified*, for example when an image characterized by black and white stripes has to be transmitted. There, we have several consecutive and identical symbols to be transmitted, so reflecting in LEDs on the same power level for several time instants, including the level zero corresponding to the source switch off. It is worth specifying that I_0 and $s_n(t)$ represent current signals that, by assuming ideal electro-optical conversion at transmit side, define the optical signal $x(t)$. Still regarding eq. (3), A_m is one of the M amplitudes belonging

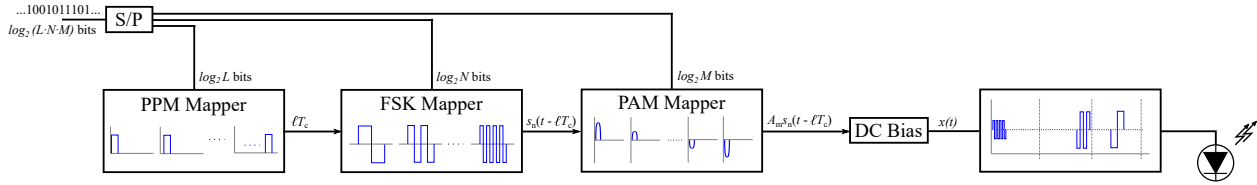


Fig. 2. Block diagram of the PPM-FSK-PAM modulator.

to the PAM-based alphabet $\mathcal{A} = \{A_0, A_1, \dots, A_{M-1}\}$, T_c is the elementary PPM-like delay and the index $\ell = 0, 1, \dots, L-1$ rules the signal time shift according to one of the L possible PPM delays gathered in $\mathcal{L} = \{0, T_c, \dots, (L-1)T_c\}$. Finally, $s_n(t)$ is the square wave describing the N -FSK signal shape, with $n=1, 2, \dots, N$ indicating the number of wave cycles within the signaling time T_p . In detail, $s_n(t)$ can be represented as:

$$s_n(t) = \sum_{k=1}^n \left(\text{rect} \left(\frac{t - T_p/4n - (k-1)T_p/2n}{T_p/2n} \right) - \text{rect} \left(\frac{t - T_p/4n - kT_p/2n}{T_p/2n} \right) \right) \quad (4)$$

where the first term is the positive portion of the square wave and the second term represents the negative component of the square wave. The modulator combining the principles of PPM, FSK and PAM signaling is depicted in Fig. 2, while a graphical example of symbol emission is reported in Fig.3. Once more, it is possible to appreciate that the symbol power is constant, hence, the illumination has a constant value on a symbol basis. Given T_c and T_p , the use of L possible delays, N possible frequencies and M possible amplitudes entails the overall symbol time to be equal to $T_s = T_p + (L-1)T_c$ (it is worth clarifying that the PAM modulation does not impact on the symbol duration, but only on amplitude). Interestingly, it can be noted that if $T_c = T_p$ the orthogonal PPM signaling is realized, while $T_c < T_p$ returns non-orthogonal PPM. In this direction, by expressing $T_c = \beta T_p$, with $0 < \beta \leq 1$ ($\beta = 1$ representing orthogonal PPM), the spectral efficiency of the proposed modulation format (related to the electrical signal) is given by:

$$\eta = \frac{\log_2(L \cdot N \cdot M)}{N(1 + \beta(L-1))}. \quad (5)$$

According to the modulator block diagram in Fig. 2, the bit mapping can be done by composing the bit string related to the generic symbol as $\log_2(L \cdot M \cdot N)$ bits where the first $\log_2 L$ are related to PPM, the second $\log_2 N$ are linked to FSK and the last $\log_2 M$ deal with PAM.

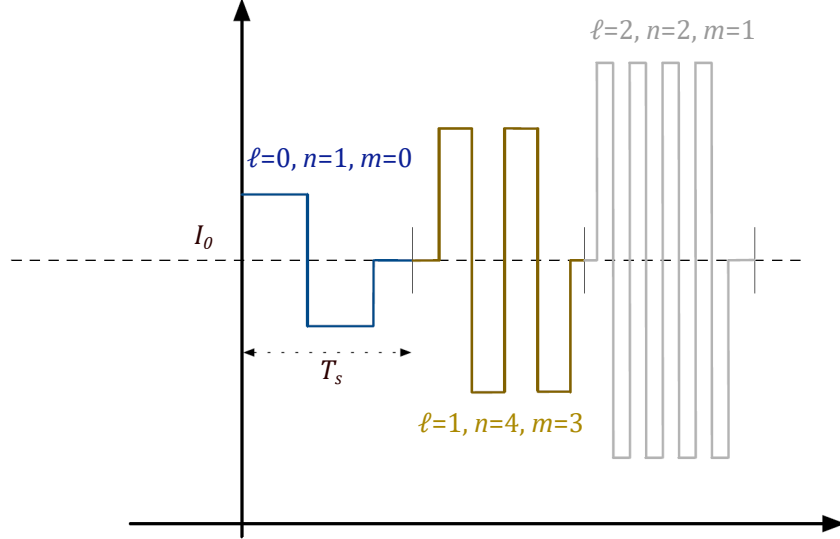


Fig. 3. Graphical representation of modulated symbols with different combinations of ℓ , n and m .

160 It is worth highlighting that the proposed scheme combines a highly spectrally efficient
 161 modulation such as PAM with spectrally inefficient but reliable modulation like PPM and FSK.
 162 In this regard, PPM and FSK realize a sort of coding (even though here no channel coding
 163 is present) as they provide a higher robustness to errors with respect to pure PAM signaling,
 164 that is unavoidably paid in terms of spectral efficiency reduction. In fact, by looking at eq. (5),
 165 the use of PAM signaling ($M > 1$) allows η to increase, while the presence of PPM and FSK
 166 ($L > 1$, $N > 1$) lowers η . Moreover, β ruling the width of PPM delay impacts on the trade off
 167 between spectral efficiency and reliability as well. Another interesting aspect to highlight is that,
 168 by smartly combining the three different techniques, we are able to improve energy efficiency. In
 169 particular, energy efficiency is meant as the system is able to reduce the BER in correspondence
 170 to the same SNR values, thus requiring lower power to achieve the same performance of other
 171 schemes.

172 III. DIGITAL DEMODULATION: OPTIMAL AND SUB-OPTIMAL RECEIVERS

173 As detailed in the previous section, by combining PPM, FSK and PAM we realize a multi-
 174 dimensional modulation scheme jointly exploiting time, frequency and amplitude domains. Re-
 175 garding digital demodulation, we must anticipate that the relationship that links PPM, FSK and
 176 PAM still holds. In fact, a possible wrong decision about the PPM part of the symbol may induce

177 errors both in symbol frequency and amplitude detection. An unreliable decision on the FSK part
 178 may lead PAM detection to be unreliable as well. Finally, having many close signal amplitudes
 179 available makes PAM detection very challenging, and errors may have also a significant impact
 180 on PPM symbol part recognition.

181 Such a *circular* dependency among PPM, FSK and PAM suggests that *parallel detection* of
 182 the three modulation components can not be followed. Therefore, a different approach combining
 183 time, frequency and amplitude dimensions is required. In this regard, we resort to the principles
 184 of Maximum Likelihood (ML) criterion allowing symbol detection to be described as follows.
 185 First, the transmit signal model in eq. (3) allows eq. (1) to be rewritten as:

$$y(t) = \rho h I_0 + \rho h A_m s_n(t - \ell T_c) + w(t) \quad (6)$$

186 from which it is possible to recover the unbiased continuous time received signal as:

$$y_u(t) = y(t) - \rho \tilde{h} I_0 = \rho h A_m s_n(t - \ell T_c) + w(t) \quad (7)$$

187 where the term \tilde{h} is the estimated version of the channel that, under the hypothesis of reliable
 188 estimation, leads to have the $y_u(t)$ with zero-mean. As previously outlined, the bits carried by
 189 PPM, FSK and PAM must be decoded in a joint fashion. The most effective, but also expensive,
 190 way to achieve this goal is to implement the so called optimum receiver (OR) [19], based
 191 on signal filtering operated by considering all the possible combinations of PPM, FSK and
 192 PAM signals. As alternatives, we present three sub-optimal receivers, referred as quasi-optimum
 193 receiver (QOR), direct receiver (DR) and feedback receiver (FBR), respectively. Below, we
 194 detail the characteristics of the mentioned receivers, discussing the different trade off between
 195 complexity and performance provided by each configuration.

196 A. Optimum receiver

197 By looking at the scheme of the OR reported in Fig. 4 (excluding the gray section), it is
 198 possible to appreciate that, by employing L -PPM and N -FSK, $L \cdot N$ filters matched to different
 199 delays and frequencies are required in order to evaluate the corresponding $L \cdot N$ decision metrics,
 200 given as:

$$r_{\ell,n} = \frac{1}{T_p} \int_{\ell T_c}^{\ell T_c + T_p} y_u(t) s_n(t - \ell T_c) dt \quad (8)$$

with $n=1,\dots,N$, $\ell=0,\dots,L-1$. Then, the decision related to the PPM-FSK symbol components is taken according to the following rule, that allows to obtain the pair $(\hat{\ell}, \hat{n})$:

$$\hat{\ell}, \hat{n} = \underset{\ell=0,\dots,L-1, n=1,\dots,N}{\operatorname{argmax}} |r_{\ell,n}|. \quad (9)$$

representing the indexes of the decided PPM and FSK symbols, respectively. It is important to highlight that, in eq. (9), we introduce the use of modulus on $r_{\ell,n}$ since the electrical signal, for what concerns the amplitude, can be negative due to the presence of noise. Differently, measuring only the maximum on $r_{\ell,n}$ may lead to totally misdetect the frequency component.

At this stage, once decided $\hat{\ell}$ and \hat{n} , only the PAM component still needs to be detected. Hence, by resorting to the ML criterion based on Euclidean distance, we can perform the PAM detection according to the following rule:

$$\hat{m} = \underset{m=0,\dots,M-1}{\operatorname{argmin}} (\rho\tilde{h}A_m - r_{\hat{\ell},\hat{n}})^2 \quad (10)$$

so that $\hat{\ell}$, \hat{n} and \hat{m} return the decided indexes of the PPM, FSK and PAM symbols composing the transmitted multi-dimensional symbol.

Summarizing, we can define the computational cost required by the OR as $\mathcal{O}_{\text{OR}} = L \cdot N + M$, given by the $L \cdot N$ filtering operations related to PPM and FSK detection plus the M metrics computations for PAM detection. As the decision on the received multi-dimensional symbol is taken by comparing it to all the possible symbols belonging to the PPM-FSK-PAM alphabet, the OR results as the best performing receiver. On the other hand, the required computational cost \mathcal{O}_{OR} may be high, especially if the modulation orders grow.

B. Quasi-optimum receiver

The block diagram of the sub-optimal QOR is the same of the OR, but including a further processing part, highlighted in the gray area in Fig. 4, realizing a very first decision stage that allows the overall signal processing to be reduced with respect to the case related to the OR. In fact, the receiver is referred as *quasi-optimum* since, whenever possible, it avoids the full computation of the filtering operations characterizing the OR. In QOR, the initial processing stage is characterized by an energy detector that computes the signal energy over the L PPM time windows characterizing the received signal $y_u(t)$. So, we have that the quantity:

$$\xi(\ell) = \int_{\ell T_c}^{\ell T_c + T_p} |y_u(t)|^2 dt, \quad \ell = 0, \dots, L-1 \quad (11)$$

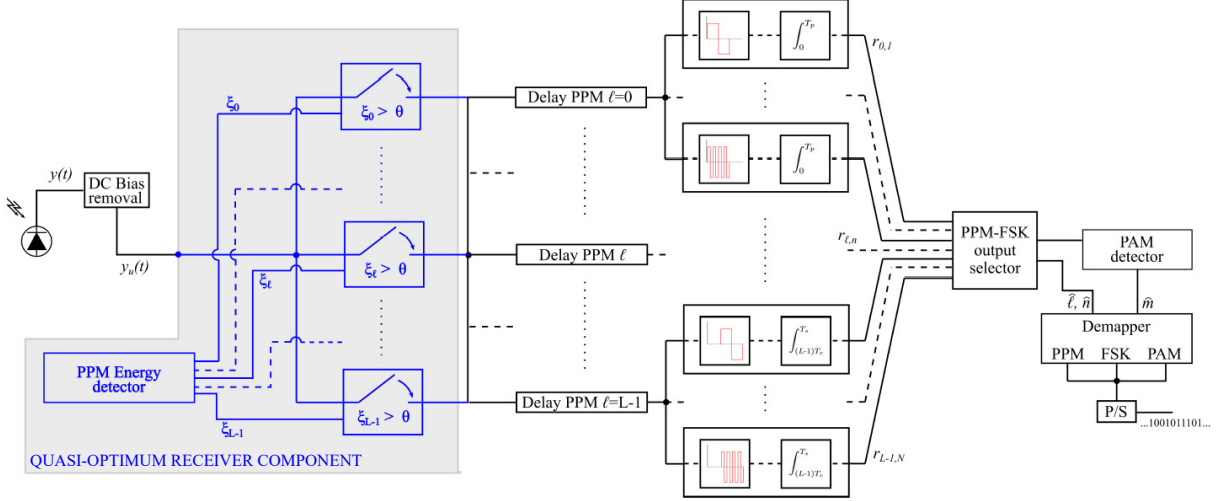


Fig. 4. Block diagram of optimum receiver (OR) and quasi-optimum receiver (blue QOR).

226 represents the signal energy referred to the ℓ -th PPM slot measured in $y_u(t)$. Once the L energy
 227 metrics are calculated, a threshold θ is used to determine the best candidates to be the detectable
 228 PPM symbols, gathered in the set $\mathcal{L}_\theta = \{\ell \mid \xi(\ell) > \theta\}$. Hence, the PPM-FSK symbol is detected
 229 according to the following rule:

$$\hat{\ell}, \hat{n} = \underset{\ell \in \mathcal{L}_\theta, n=1, \dots, N}{\operatorname{argmax}} |r_{\ell, n}| \quad (12)$$

230 where the maximum is not searched in the set characterized by $L \cdot N$ elements (as done in
 231 the optimum receiver case), but in a number of $|\mathcal{L}_\theta| \cdot N$. Please notice that, in this case, the
 232 operator $|\cdot|$ applied to the set $|\mathcal{L}_\theta|$ means its cardinality, that is, the number of elements that it
 233 is composed of. As in general $\mathcal{L}_\theta \leq L$, the number of metrics computed according to eq. (8) is
 234 lower in QOR than in the optimal receiver, thus saving computational effort.

235 The setup of the threshold θ depends on the energy level expected to be measured within
 236 the PPM slot where the FSK signal is placed on. In this regard, let us assume the transmission
 237 of a pilot multi-dimensional symbol $x_p(t)$ where ℓ , n and m are known. The estimated energy,
 238 calculated as in eq. (11) in the ℓ -th PPM slot and referred as ξ_p , can be exploited to define the
 239 threshold theta as $\theta = (1 - \beta)\xi_p$, that essentially represents the energy level expected in the
 240 $(\ell + 1)$ -th PPM slot immediately next to that one where the signal is placed on. In fact, due to

241 their closeness, the ℓ -th PPM symbol is likely to be confused with the $(\ell + 1)$ -th one, so this is
 242 why the threshold θ is set as a function of the energy expected on the $(\ell + 1)$ -th PPM slot.

243 Finally, concerning the detection of the PAM symbol, we proceed in the same way reported
 244 in eq. (10). Overall, the processing cost related to the QOR is $\mathcal{O}_{\text{QOR}} = L + \mathcal{L}_\theta \cdot N + M$, given
 245 by the L filtering operations characterizing the PPM energy detector, $\mathcal{L}_\theta \cdot N$ filters for PPM and
 246 FSK detection, and finally M metrics computations related to PAM decision. It is worth noting
 247 that \mathcal{O}_{QOR} is not a fixed value since it strongly depends on the number of elements composing
 the set \mathcal{L}_θ .

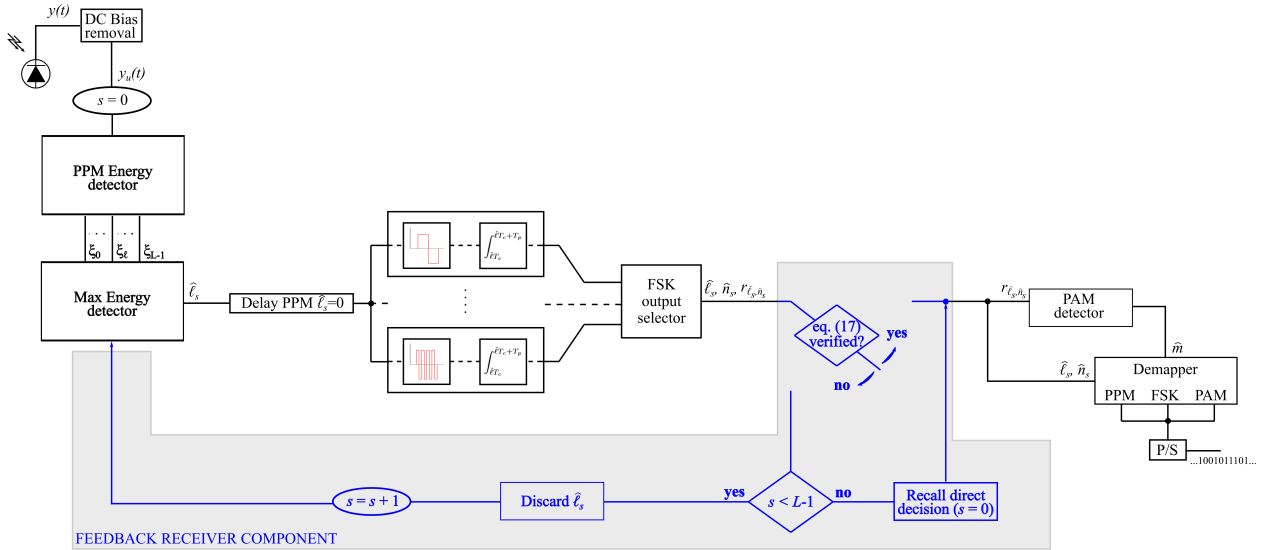


Fig. 5. Block diagram of direct receiver (DR) and feedback receiver (FBR).

248

249 C. Direct receiver

250 The receiver introduced as DR is probably the less complex sub-optimal solution in terms
 251 of computational cost since signal detection is performed sequentially, starting from the PPM-
 252 related part, then moving to FSK and finally to PAM parts. The use of such detection approach
 253 is the reason why the receiver is referred as *direct*. For the sake of clarity, we would remark that,
 254 in this case, detection is not operated jointly on the PPM, FSK and PAM signal components. The
 255 block diagram of DR is depicted in Fig. 5 (excluding the gray box). Regarding PPM detection,
 256 an energy detector as that one introduced in eq. (11) is considered, so as:

$$\hat{\ell} = \max_{\ell=0, \dots, L-1} \xi(\ell) \quad (13)$$

257 returns the index of the decided symbol related to the PPM part. From $\hat{\ell}$ it is possible to identify
 258 the time delay characterizing the FSK signal $s_n(t)$ within the received symbol $y_u(t)$, so that the
 259 FSK detection can be performed according to the following rule:

$$\hat{n} = \operatorname{argmax}_{n=1,\dots,N} |r_{\hat{\ell},n}| \quad (14)$$

260 where it is important to highlight that we are not dealing with $r_{\ell,n}$ as in eq. (8), but with $r_{\hat{\ell},n}$
 261 defined as:

$$r_{\hat{\ell},n} = \frac{1}{T_p} \int_{\hat{\ell}T_c}^{\hat{\ell}T_c+T_p} y_u(t) s_n(t - \hat{\ell}T_c) dt. \quad (15)$$

262 In other words, eq. (15) defines the filtering operations that consider only the specific time delay
 263 given by $\hat{\ell}$, while filtering in eq. (8) is performed for $\ell=0,1,\dots,L-1$. Finally, for what concerns
 264 PAM detection, we can still resort to the ML based approach followed in eq. (10).

265 Regarding the DR, the number of filtering operations and comparisons requested for symbol
 266 demodulation is really low since, as previously outlined, detection is performed sequentially on
 267 the PPM, FSK and PAM parts. Therefore, the required computational cost is given as $\mathcal{O}_{\text{DR}} =$
 268 $L + N + M$.

269 *D. Feedback receiver*

270 The last receiver we propose is referred as FBR and it is somewhat similar to the DR. In fact,
 271 its reference block diagram is that one reported in Fig. 5, but including the gray area as well.
 272 With FBR, it is possible to take a temporary decision on the PPM-FSK symbol part, with the
 273 detection being potentially performed multiple times iteratively. Therefore, as highlighted in Fig.
 274 5, a feedback-like mechanism is realized and integrated in the DR architecture. In this regard,
 275 we indicate the iteration number with the subscript s , so that $\hat{\ell}_s$ refers to the PPM symbol part
 276 decided at the s -th detection iteration. For $s=0$, we have the very first decision on PPM as taken
 277 according to eq. (13) similarly to the DR case. Even for FSK detection, for $s=0$, \hat{n}_s is determined
 278 as in eq. (14) representing the maximum output of matched filtering. Differently from DR, we
 279 also consider a second potential candidate to be the decided FSK symbol, formally defined as:

$$\hat{n}_s^\diamond = \operatorname{argmax}_{n \in \mathcal{N}/\{\hat{n}_s\}} |r_{\hat{\ell},n}| \quad (16)$$

that is the second-highest output of eq. (15) (in other words, maximum output of matched filtering excluding \hat{n}_s). Given such two candidates, \hat{n}_s is recognized as a reliable decision if the following conditions are simultaneously met:

$$|r_{\hat{\ell}_s, \hat{n}_s}| - |r_{\hat{\ell}_s, \hat{n}_s^\diamond}| > \Psi \quad (17a)$$

$$|r_{\hat{\ell}_s, \hat{n}_s}| > \Gamma. \quad (17b)$$

Specifically, eq. (17a) is used to explicitly verify the accuracy of FSK decision. In fact, if the difference between \hat{n}_s and \hat{n}_s^\diamond is larger than a suitably defined threshold Ψ , it follows that the computing of N matched filters returns an output, namely \hat{n}_s , significantly higher than the others. So, it is likely that \hat{n}_s correctly identifies the index of the received FSK symbol. The reference threshold is defined as $\Psi = 0.25(A_{M-1} - A_0)/(M - 1)$ and is function of the distance expected between adjacent PAM amplitudes, with 0.25 being an empirically chosen scaling factor. Eq. (17b) allows not only to explicitly verify the reliability of FSK detection, but also to understand if the decision on PPM has been taken correctly. In this regard, if the N matched filters computed for FSK detection returns very low output values, it may be that a wrong decision on PPM has led to a misaligned identification of the FSK signal within $y_u(t)$, causing the FSK filtering to be *unmatched*. On the other hand, if the highest filter output $r_{\hat{\ell}_s, \hat{n}_s}$ exceeds a certain threshold Γ , conveniently chosen to deal with energy detector behavior, it is likely that the PPM detection has been performed reliably. To this aim, the threshold has been set as $\Gamma = 0.25|A_{\min}|$, with A_{\min} being the minimum amplitude for a PAM symbol and 0.25 representing a scaling factor as for Ψ . Therefore, the joint meeting of eqs. (17a)-(17b) should prevent from a wrong decision on the PPM-FSK symbol pair $(\hat{\ell}_s, \hat{n}_s)$.

Otherwise, if eq. (17) is not met, we consider the next step for s , that is the next iteration, and we get back to the energy detection stage by evaluating:

$$\hat{\ell}_{s+1} = \max_{\ell \in \mathcal{L}/\{\hat{\ell}_0, \dots, \hat{\ell}_s\}} \xi(\ell) \quad (18)$$

that is a new decision on the PPM symbol part, but excluding the index $\hat{\ell}_s$ found during the previous iteration. Once the *new* decided PPM symbol is available, we proceed again with FSK detection by computing eqs. (13)-(16) and checking if, given $\hat{\ell}_{s+1}$, eq. (17) is finally met. Such procedure is repeated until eq. (17) is verified or, at most, L times corresponding to the maximum number of decisions that can be considered for PPM, thus realizing the feedback path highlighted in Fig. 5. Just in case eq. (17) is never achieved, the final symbol decision will be the one related

to the iteration $s = 0$. Finally, dealing with PAM detection, still we can resort to eq. (10).

It is important to note that in FBR, as for QOR, the number of filtering operations and symbol comparisons is not fixed since it depends on the meeting of conditions in eq. (17). Hence, the cost is $\mathcal{O}_{\text{FBR}} = L + (s + 1) \cdot N + M$ where the fixed terms L and M are related to the implementation of the PPM energy detector and PAM detector, respectively, while the remaining variable term is function of the number of feedback iterations.

Remark - about the possible receiver selection

Although the implementation of DR is worth for what concerns cost, the optimal receiver allows to achieve the minimum error rate, thus granting the highest level of reliability. Hence, the use of the most convenient receiver can be seen in two different ways. First, if the setup is fixed and it is expected that no significant changes are applied to the communication link, once assigned the parameters, it is possible to select the receiver allowing the achievement of the requested target performance in terms of error rate, while optimizing the receiver computational effort. This represents an offline solution. Second, if the channel is subject to variations (for example a user moving in a room), the received optical power changes and so the signal-to-noise ratio (SNR). This implies that, if the receiver is implemented by software, it is possible to realize a SNR threshold based detection method tuning, so that the channel conditions drive the most convenient receiver selection. By doing so, the requested reliability level can be provided at the lowest processing cost. We comment further in the numerical results section the possible use of the receiver selection procedure.

IV. NUMERICAL RESULTS

In this section, we investigate the performance of the proposed multi-dimensional modulation scheme, highlighting the benefits brought by the use of such approach in terms of both communication reliability and illumination control. Furthermore, we evaluate the effectiveness of the three sub-optimal receivers presented in the previous section, discussing the trade off between computational complexity and error rate achievable with respect to the optimum receiver case. Matlab software was employed for simulating the transmission of 10^7 symbols over a point-to-point optical link. In addition, some results obtained from experimental validation are also reported and discussed. Different communication distances between transmitter and receiver have

334 been considered so as to investigate the performance as a function of the average electrical SNR
 335 per symbol, formally defined as:

$$\gamma = \frac{1}{K_s} \sum_{i=0}^{K_s-1} \frac{(\rho P_i h)^2}{\sigma_w^2} \quad (19)$$

336 where $K_s = L \cdot N \cdot M$ is the size of the considered multi-dimensional modulation vocabulary
 337 and P_i is the power of the i -th transmitted symbol, with $i = 0, 1, 2, \dots, K_s-1$. For simulations, we
 338 considered normalized LED and PD parameters since performance are evaluated as a function
 339 of SNR. On the other hand, a detailed description of hardware parameters and setup is provided
 340 when presenting the experimental results.

341 A. Optimum and Multi-dimensional modulation performance

342 As outlined in Sec. II, the multi-dimensional modulation allows the high spectral efficiency
 343 of PAM to be combined with the reliability of PPM and FSK, to achieve good data rates while
 344 providing robustness to errors. In this direction, we now compare the BER performance of
 345 uncoded and coded PAM with some PPM-FSK-PAM schemes.

346 **Comparison with uncoded strategy:** We selected some modulation formats providing a target
 347 spectral efficiency $\eta^*=1$ bit/s/Hz and $\eta^*=2$ bit/s/Hz achieved with 2-PAM (or OOK) and 4-PAM,
 348 respectively. Such PAM formats have been taken as a reference since being the most widespread
 349 in OWCS [21], [22]. In fact, the optical signal starts suffering from high attenuation after few
 350 decades of centimeters propagation, therefore using higher order PAM modulations results as
 351 unreliable due to the detection errors caused by the presence of noise.

352 Given $\eta^*=1$ bit/s/Hz, 2-PAM has been compared to 2-PPM/2-FSK/2-PAM with $\beta=0.5$, to 4-
 353 PPM/2-FSK/4-PAM with $\beta=0.5$ and to 16-PPM/4-FSK/2-PAM with $\beta=0.05$. The BER results
 354 are plotted in Fig. 6(a), with curves related to the multi-dimensional modulations being obtained
 355 considering the OR based detection. In particular, it can be appreciated that the multi-dimensional
 356 modulations characterized by 16-PPM/4-FSK/2-PAM and 2-PPM/2-FSK/2-PAM are able to out-
 357 perform 2-PAM, while 4-PPM/2-FSK/4-PAM provide worse performance. Such results can be
 358 explained as follows. By recalling eq. (5), the use of PPM and FSK (that is, $L > 1$ and $N > 1$)
 359 lowers the spectral efficiency. So, there is a limited number of combinations of L , N and β that
 360 guarantee the achievement of the target η^* . Moreover, the spectral efficiency reduction caused
 361 by the use of PPM and FSK must be counterbalanced by increasing the PAM modulation order
 362 as well. This is what happens when dealing with the considered 4-PPM/2-FSK/4-PAM case.

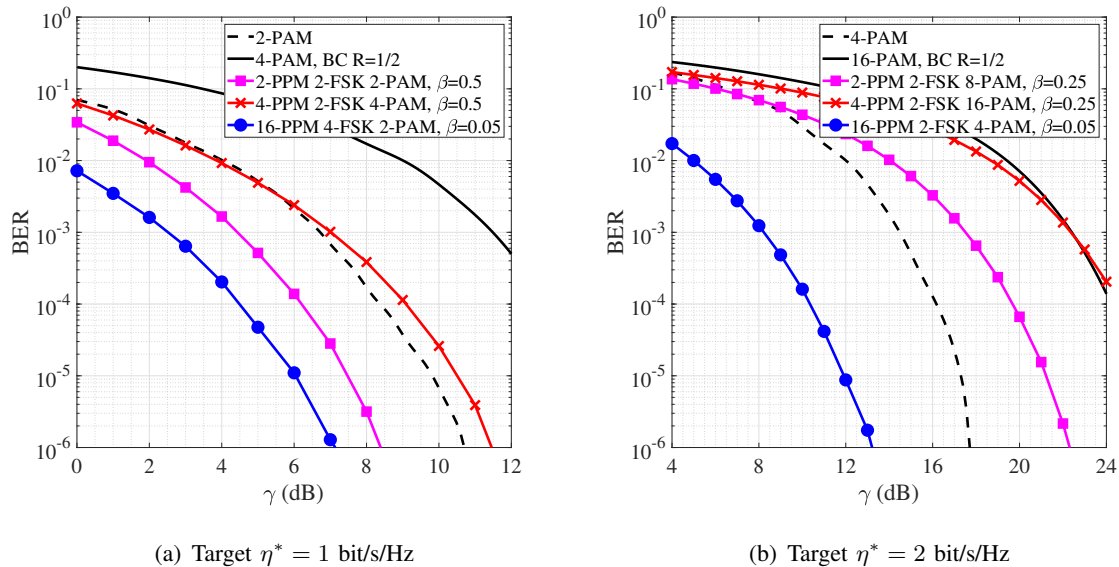


Fig. 6. BER performance, based on the OR, of different modulation schemes providing the same spectral efficiency η^* .

363 Unfortunately, the use of PPM and FSK to achieve a higher reliability requests the PAM order
 364 M to be increased up to 4 so as to guarantee $\eta^*=1$ bit/s/Hz. Hence, the benefits brought by PPM
 365 and FSK in terms of robustness to errors are *lost* since the use of 4-PAM leads the communication
 366 to be more sensitive to errors than an uncoded 2-PAM. As a consequence, such kind of multi-
 367 dimensional modulation is not convenient with respect to 2-PAM.

368 Moving to a more challenging case, Fig. 6(b) shows the BER for those schemes providing
 369 a target spectral efficiency $\eta^*=2$ bit/s/Hz, that are uncoded 4-PAM, 2-PPM/2-FSK/8-PAM with
 370 $\beta=0.25$, 4-PPM/2-FSK/16-PAM with $\beta=0.25$ and to 16-PPM/2-FSK/4-PAM with $\beta=0.05$. Curves
 371 still refer to the performance achieved with the OR. Even in this case, it can be observed that
 372 2-PPM/2-FSK/8-PAM and 4-PPM/2-FSK/16-PAM are not feasible since the introduction of PPM
 373 and FSK requires the increase of the PAM order to achieve the desired spectral efficiency. So,
 374 as discussed before, the benefits of PPM and FSK are *canceled* by the use of an unreliable PAM
 375 order.

376 **Comparison with coded strategy:** An easy comment and objection is that, in order to grant
 377 reliability, a coding strategy may be applied, obviously at the cost of spectral efficiency reduction
 378 since a part of the bits sent on the channel are for error correction. In this regard, we proceed
 379 with an additional performance comparison that is related to block coding (BC) with coding rate
 380 $R=1/2$, thus meaning that the ratio between the number of bits entering in the coder are half of

381 the ones out the coder. In order to provide a comparison for the same spectral efficiency $\eta^*=1$
 382 bit/s/Hz, we considered 4-PAM. As just mentioned, the role of channel coding is to improve
 383 the robustness to errors, but at the expense of rate reduction. Therefore, the achievement of the
 384 target spectral efficiency requests the PAM order to be necessarily increased. From the results,
 385 we can appreciate that the performance of coded 4-PAM are significantly lower than uncoded
 386 2-PAM, thus revealing that the proposed multi-dimensional modulation is more convenient than
 387 coding. Of course, many other coding schemes may be considered, but the achievement of
 388 good performance unavoidably requires the decoding strategy complexity increase. Differently,
 389 in 16-PPM/4-FSK/2-PAM with $\beta=0.05$ and 2-PPM/2-FSK/2-PAM with $\beta=0.5$ the PAM order
 390 remains the lowest possible, while PPM and FSK are introduced to achieve a higher reliability. In
 391 fact, these solutions result as better performing than uncoded 2-PAM even though providing the
 392 same spectral efficiency. In Fig. 6(b), the same problem concerns 16-PAM with block coding
 393 and $R=1/2$, where the unreliability of the high PAM modulation order can not be properly
 394 counterbalanced by coding. On the other hand, the implementation of a 16-PPM/2-FSK/4-PAM
 395 results to be more convenient than an uncoded 4-PAM, thus meaning that PPM and FSK are
 396 exploited fruitfully to achieve a lower BER.

397 *Results Discussion*

398 Interestingly, it can be noted from Fig. 6 that the most reliable modulation schemes to achieve
 399 both $\eta^*=1$ bit/s/Hz and $\eta^*=2$ bit/s/Hz consider the use of a high PPM order equal to $L=16$,
 400 that may induce a significant spectral efficiency decrease according to eq. (5). However, in both
 401 cases we have $\beta=0.05$ allowing the realization of a non-orthogonal PPM, which provides a
 402 lower spectral efficiency reduction with respect to orthogonal PPM (where $\beta=1$). Furthermore,
 403 it is worth highlighting that, in general, when dealing with the proposed multi-dimensional
 404 modulation, using high PPM modulation formats may be more convenient than increasing the
 405 FSK order. In fact, regarding PPM, we have two degree of freedom to adjust the spectral
 406 efficiency, that are L and β . On the other hand, FSK performance are ruled by the unique
 407 parameter N . Hence, by increasing N the spectral efficiency decreases, but there is no other
 408 way to mitigate such reduction, as happens in PPM by adjusting β .

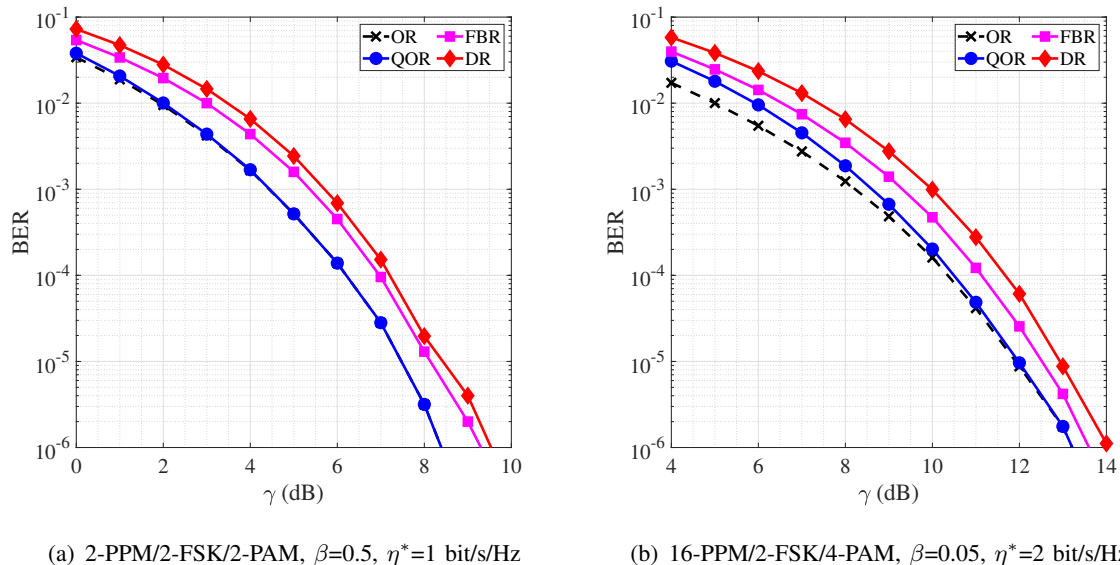


Fig. 7. BER performance of different multi-dimensional modulations with optimal and sub-optimal receivers.

410 B. Trade off between computational complexity, spectral efficiency and error rate

411 Once identified the most suitable multi-dimensional modulation formats allowing the achieve-
 412 ment of the considered target spectral efficiency, we pass now to investigate the performance of
 413 the proposed sub-optimal receivers. The results are still shown in terms of BER as a function of
 414 the SNR. Dealing with $\eta^*=1$ bit/s/Hz, Fig. 7(a) is related to 2-PPM/2-FSK/2-PAM with $\beta=0.5$,
 415 while Fig. 7(b) describes the performance of 16-PPM/2-FSK/4-PAM with $\beta=0.05$, related to
 416 $\eta^*=2$ bit/s/Hz. We have chosen such two modulation formats since characterized by different
 417 values of L , N and M that can impact on the receiver performance. For what concerns 2-PPM/2-
 418 FSK/2-PAM, Fig. 7(a) shows that QOR and OR guarantee the same reliability level, with the
 419 performance of FBR and DR being very close as well. This is due to the fact that, since L , N
 420 and M are equal to the lowest order possible, that is 2, the number of transmittable symbols
 421 is the lowest possible as well, hence reliability performance are less sensitive to the detection
 422 mechanism type. Regarding 16-PPM/2-FSK/4-PAM, as depicted in Fig. 7(b), the sub-optimal
 423 receivers still provide performance close to the optimum one. In this case where $\eta^*=2$ bit/s/Hz,
 424 symbol detection results as more challenging than for the previously investigated schemes.
 425 Therefore, having similar performance between optimal and sub-optimal solutions allows the
 426 receiver selection to be potentially performed basing on the computational effort constraints.

427 Following the remarks presented in Section III about the receiver selection, by means of the

TABLE I
COMPUTATION COST FOR QOR AND FBR.

Modulation scheme	Subopt. receiver	SNR γ			
		3 dB	6 dB	9 dB	12 dB
2-PPM/2-FSK/2-PAM $\beta = 0.5$	QOR	1.15	1.15	1.15	1.16
	FBR	1.01	1.00	1.00	0.99
16-PPM/4-FSK/2-PAM $\beta = 0.05$	QOR	0.49	0.47	0.46	0.45
	FBR	0.37	0.34	0.33	0.33
16-PPM/2-FSK/4-PAM $\beta = 0.05$	QOR	0.70	0.69	0.67	0.65
	FBR	0.64	0.63	0.61	0.61

428 proposed scheme we have the capability to select the most appropriate scheme to guarantee
 429 the quality of service achievement based on the propagation conditions, while selecting the less
 430 expensive approach from a computational point of view. In this direction, in order to evaluate the
 431 computational effort required by the proposed sub-optimal receivers with respect to the optimum
 432 one, we introduce now the metric $\mathcal{C}_d = \mathcal{O}_d/\mathcal{O}_{\text{OR}}$, measuring the processing effort required by
 433 the d -th receiver type ($d = \text{QOR,DR,FBR}$), normalized to the optimum receiver computational
 434 cost.

435 As discussed in Sec. III-C, the computational cost related to DR is fixed since depending
 436 only on L, N, M . Hence, for 2-PPM/2-FSK/2-PAM, 16-PPM/4-FSK/2-PAM and 16-PPM/2-
 437 FSK/4-PAM we have that $\mathcal{C}_{\text{DR}}=1$, $\mathcal{C}_{\text{DR}}=0.333$ and $\mathcal{C}_{\text{DR}}=0.611$, respectively. This means that, when
 438 dealing with 2-PPM/2-FSK/2-PAM, the processing complexity required by the DR is essentially
 439 the same of the OR, while for the cases 16-PPM/4-FSK/2-PAM and 16-PPM/2-FSK/4-PAM
 440 the use of DR allows a significant computational effort saving of about 70% and 40% with
 441 respect to the OR, respectively. On the other hand, the performance of QOR and FBR depends
 442 on the SNR impacting on eq. (12) and eq. (17). In this regard, Table I reports the results
 443 related to the considered QOR and FBR, measured at different SNR levels, and considering
 444 2-PPM/2-FSK/2-PAM, 16-PPM/4-FSK/2-PAM and 16-PPM/2-FSK/4-PAM resulted as the best
 445 performing schemes from the previous analysis. Interestingly, it can be noted that, when dealing
 446 with 2-PPM/2-FSK/2-PAM, the sub-optimal receivers seem to be more costly than the optimum
 447 one. Such result is explained by the fact that, since $L=2$, the filtering operations for PPM-FSK
 448 detection required by QOR and FBR are essentially the same as for the OR. In fact, for QOR we

449 have that L_θ can be 1 or 2, thus very close or equal to L , while in FBR the running of a single
 450 feedback iteration leads the computational cost to be essentially the same as in the optimum
 451 case. Moreover, both QOR and FBR consider the implementation of an energy detector as initial
 452 stage of processing, that is not present in the OR. So, this is the reason why \mathcal{C}_{QOR} and \mathcal{C}_{FBR} are
 453 greater or equal to 1. Moving to 16-PPM/4-FSK/2-PAM and 16-PPM/2-FSK/4-PAM where L is
 454 very large, the processing saving provided by QOR and FBR (despite the implementation of the
 455 PPM energy detector) becomes remarkable since, in general, in QOR L_θ may be much smaller
 456 than L and in FBR the feedback iterations may be few. Specifically, in 16-PPM/4-FSK/2-PAM
 457 the cost of QOR is less than half of that one referred to the OR, while the cost of DR is even
 458 lower, with processing saving being larger than 60%. In the case of 16-PPM/2-FSK/4-PAM,
 459 representing a higher performing modulation since providing a spectral efficiency equal to 2
 460 bit/s/Hz, the computational effort requested by QOR and DR increases. However, more than
 461 30% of processing is avoided with respect to the OR case, and this result is still significant.
 462 Furthermore, the computational cost characterizing QOR and FBR tends to lower as the SNR
 463 grows, even though such decrease is only slight. In this regard, both 16-PPM/4-FSK/2-PAM
 464 and 16-PPM/2-FSK/4-PAM consider a very small β , so it follows that the PPM energy detector
 465 returns L values that are comparable in amplitude since PPM is far from be orthogonal. Hence,
 466 the number of filtering operations for QOR and FBR may not be the minimum one. On the other
 467 hand, by enlarging β the PPM detection results more reliable. As a consequence, in QOR L_θ
 468 tends to 1 and in FBR the feedback becomes rarely necessary (thus leading to the performance
 469 of DR).

470 Till now, we have slightly discussed about the role of β , anyway it is important to deeply
 471 explain its impact. As previously outlined, the use of a high PPM order as for 16-PPM/4-FSK/2-
 472 PAM and 16-PPM/2-FSK/4-PAM is made possible thanks to the realization of a non-orthogonal
 473 signaling with $\beta \ll 1$, allowing the spectral efficiency reduction due to L to be mitigated. By
 474 referring to the considered schemes, we now show in Fig. 8 how the choice of β rules the trade
 475 off between BER and spectral efficiency. Results have been obtained at $\gamma=2.5$ dB and $\gamma=8$ dB
 476 for 16-PPM/4-FSK/2-PAM and 16-PPM/2-FSK/4-PAM, respectively, which represent the SNR
 477 conditions where a BER equal to 10^{-3} is achieved (see Fig. 6). Specifically, each point in Fig.
 478 8 is characterized by a unique x coordinate, related to BER, and a double y coordinate related
 479 to β and η . Here, β is the independent variable (that is reported on the y -axis instead of the
 480 x -axis as in conventional plotting), while BER and η are the dependent ones. In fact, according

481 to eq. (5), there is a direct relationship between the values reported in the left y -axis (β) and
 482 in the right one (η) of Fig. 8. Furthermore, β impacts also on the reliability of PPM detection
 and on BER, reported on the x axis. By referring to Fig. 8(a) describing the performance of

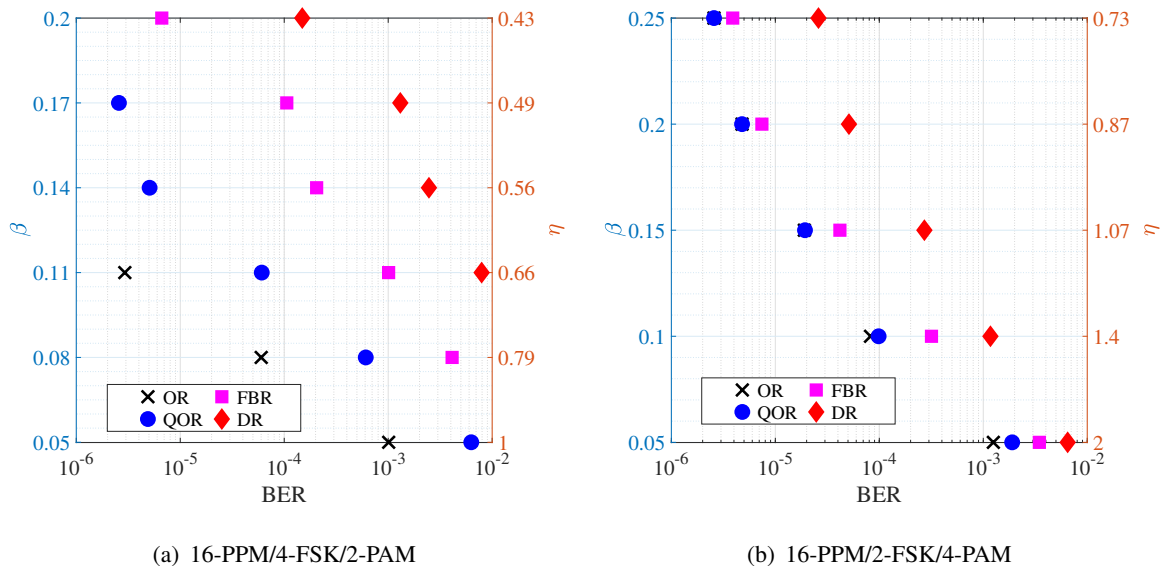


Fig. 8. Performance trade off between BER and η^* as a function of β .

483

484 16-PPM/4-FSK/2-PAM providing $\eta^*=1$ bit/s/Hz, it is possible to appreciate that, for whatever
 485 detection mechanism employed at the receiver, BER lowers as β grows. When dealing with OR
 486 and QOR, the high reliability of the considered detection approaches allows the use of $\beta < 0.15$
 487 to achieve a BER below 10^{-5} . On the other hand, for FBR and DR representing less complex
 488 solutions, a larger β would be required for performance improvement. Moving to the case
 489 16-PPM/2-FSK/4-PAM providing $\eta^*=2$ bit/s/Hz, the performance of all the considered receivers
 490 follows essentially a similar behavior, with BER below 10^{-5} achievable only for $\beta > 0.2$. Of
 491 course, it can be verified from the right y -axis on Fig. 8 that the increase of β to improve the
 492 communication reliability is unavoidably paid in terms of spectral efficiency.

493 We recall that the main goal of our approach is to combine the robustness of PPM and FSK
 494 with the high spectral efficiency of PAM. By doing so, a more reliable communication can
 495 be achieved, without excessively sacrificing the data rate. This is what typically happens when
 496 coding is applied, with overhead being introduced to protect data from propagation errors, but
 497 by reducing rate. In this direction, we provide now a comparison with some multi-dimensional
 498 modulations and coded PAM schemes. Specifically, we considered BC with $R=1/2$ and $R=1/3$

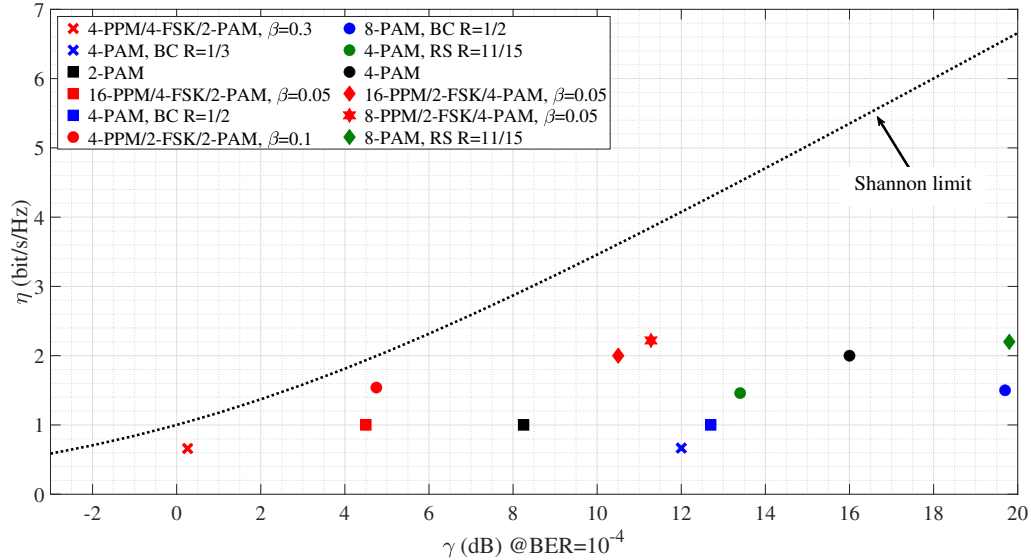


Fig. 9. Performance comparison between multi-dimensional schemes and coded modulations.

499 and Reed-Solomon (RS) coding with $R=11/15$, representing the most widespread techniques
500 providing a good trade off between effectiveness and error protection complexity. Given the
501 reference BER equal to 10^{-4} , we show in Fig. 9 a map where the points with coordinates (γ, η)
502 describe the performance of the schemes under investigation. In Fig. 9, the multi-dimensional
503 modulations are highlighted in red, pure PAM schemes in black, PAM with BC in blue and PAM
504 with RS coding in green. Different modulation orders referred to the same scheme are instead
505 differentiated with markers. For multi-dimensional modulations, we considered the performance
506 achieved with the OR. Furthermore, Fig. 9 reports also the Shannon limit curve (note that the
507 curve has not the typical logarithmic behavior as the SNR x-axis is on the logarithmic scale),
508 so that it is possible to infer how close the modulations performance are with respect to the
509 maximum achievable. Overall, it can be seen how the proposed multi-dimensional modulations
510 outperform the other coded and uncoded PAM solutions. In fact, among same colored markers,
511 those ones referring to multi-dimensional schemes are closer to the Shannon limit (see the
512 squared red marker representing 16-PPM/4-FSK/2-PAM, the red circled marker describing 4-
513 PPM/2-FSK/2-PAM and the red star-shaped marker related to 8-PPM/2-FSK/4-PAM). This means
514 that, for a given pair of target BER and spectral efficiency to be provided, multi-dimensional
515 modulations result as better performing in terms of SNR.

516 Finally, it is worth noting that the results shown in Fig. 9 allow multi-dimensional modulations
517 and coding based solutions to be compared only from a communication point of view. Another
518 fundamental benefit brought by multi-dimensional modulation concerns illumination, since the
519 use of FSK signaling allows the average source output power to be constant, thus avoiding
520 problem of dimming and flickering. On the other hand, when using PAM, with or without coding,
521 despite the emitted symbols can be assumed as equiprobable, it is not possible to achieve lighting
522 control, that may represent a severe limitation in indoor VLC scenarios where illumination and
523 connectivity services must be simultaneously provided. To sum up the main results obtained
524 in this section, we can highlight that multi-dimensional modulation scheme allows a dynamic
525 and (computation)-cost efficient selection of the most suitable multi-dimensional scheme, with
526 an eye on the power level of the light, to guarantee light levels homogeneity for users. This
527 is a key point for deploying real-world VLC systems. In other words, with multi-dimensional
528 modulation schemes, we aim to provide the most cost-effective solution by guaranteeing the
529 quality of service imposed by the underlying applications. Another important consideration is
530 regarding the energy efficiency, since as we can observe in Fig. 9, multi-dimensional modulations
531 allow to achieve the same BER with a reduced SNR with respect to other coded and uncoded
532 schemes, or otherwise said, at the same SNR level it is possible to reduce the BER, with an
533 evident impact in terms of energy reduction. From this we can infer that the proposed modulation
534 scheme allows to achieve higher energy efficiency.

535 *C. Experimental validation*

536 In order to validate the feasibility of the proposed multi-dimensional modulation, we performed
537 several experiments by realizing an ad hoc test-bed based on Software Defined paradigm (Fig.
538 10(a)). As described in the schematic diagram in Fig. 10(d), at transmit side the test signals have
539 been generated through an Arduino 1 board, using a low level code in order to directly operate
540 on the registers of the micro-controller and so avoiding unwanted latency which could prevent
541 the correctness of the tests.

542 Data were transmitted by modulating the optical emission of a Kingbright 104500 10mm red
543 LED array. Each light is controlled by a dedicated digital output of the board and the number
544 of LED simultaneously turned on determines the output optical flux. This approach allows to
545 easily implement the PAM modulation, avoiding non linearities due to the current-optical flux
546 characteristic of the LED. Since each LED is characterized by a limited output power, the

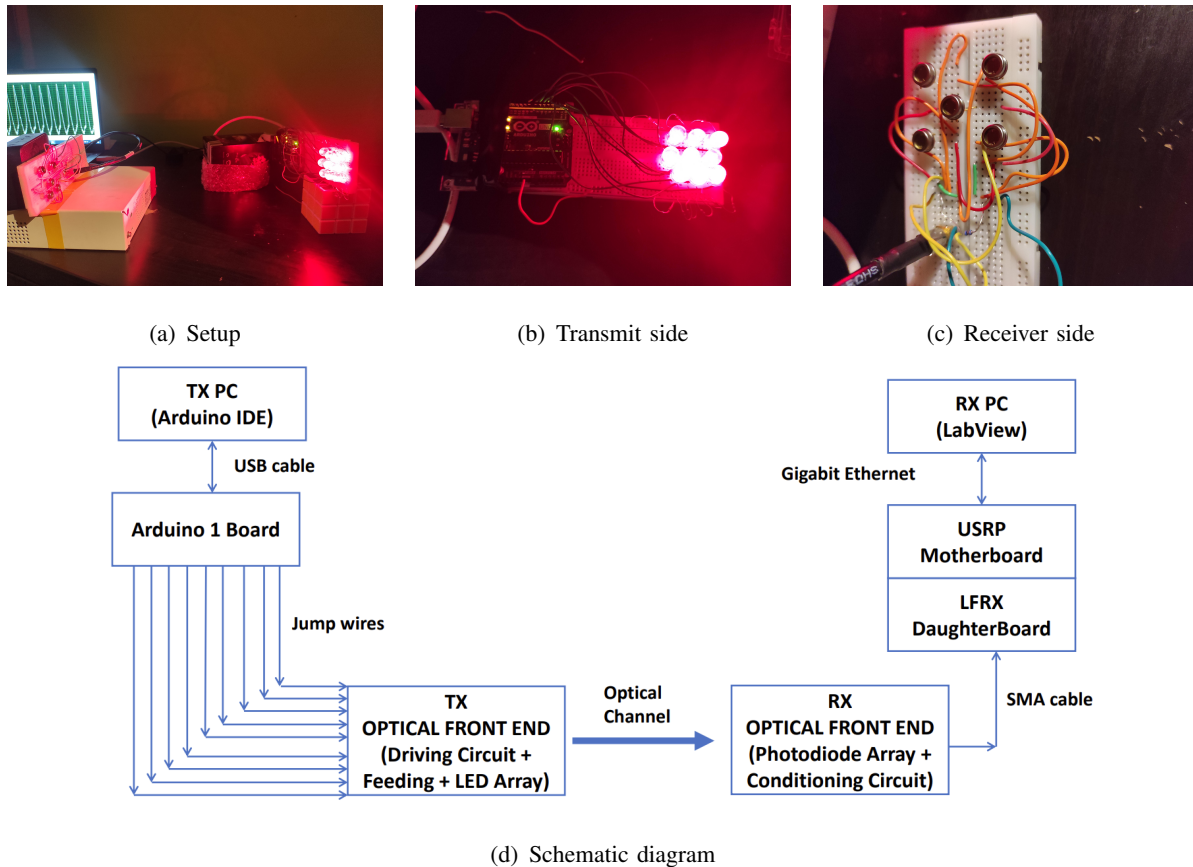


Fig. 10. Experimental setup description.

547 array configuration is also necessary to increase signal dynamics, achieve larger communication
 548 distances and maintain the proper average illumination level. In the experimental validation, we
 549 used 9 LEDs (Fig. 10(b)) in order to properly perform the PAM levels emission and generate
 550 the bias light level. At the receiver, the signal has been elaborated using a NI USRP 2920 and
 551 the commercial software LabView. In order to operate in base-band spectrum, a low frequency
 552 RX daughter-board, produced by Ettus, has been integrated between the optical receiver and
 553 the USRP motherboard. The optical receiver is composed of 5 CENTRONIC OSD15-5T PDs
 554 in order to realize a further gain and improve the quality of the received signal (Fig. 10(c)).
 555 All the PDs are arranged in parallel, acting as a unique current generator. Despite we actually
 556 realized a Multiple-Input Multiple-Output configuration, LEDs and PDs alignment has been
 557 accurately performed so as to let the system acting in Single-Input Single-Output mode. This
 558 is because using a single LED does not allow to generate reasonable power levels due to the
 559 LED characteristics (only 150mW power each). The received signal has not been amplified and

TABLE II
EXPERIMENTAL PARAMETERS

Receiver		Transmitter	
Photodiode Model	CENTRONIC OSD15-5T	LED Model	Kingbright RED 104500
Active Area	15 mm ²	Output Power	150 mW
Responsivity (620 nm)	0.4	Operative current	30 mA
Bandwidth	29.1 MHz	Light flux	1.4 lm
FOV	45°	FOV	80°
Rise time	12 ns	Forward current	30 mA

TABLE III
BER COMPARISON BETWEEN SIMULATION AND EXPERIMENT WITH OR AND QOR

Detection type	75 cm link ($\gamma=13.9$ dB)		175 cm link ($\gamma=5.6$ dB)	
	Sim.	Exp.	Sim.	Exp.
OR	$2 \cdot 10^{-7}$	$2.6 \cdot 10^{-7}$	$8.15 \cdot 10^{-3}$	$1.16 \cdot 10^{-2}$
QOR	$3.3 \cdot 10^{-7}$	$3.9 \cdot 10^{-7}$	$1.45 \cdot 10^{-2}$	$2.03 \cdot 10^{-2}$

560 no filtering operations have been performed. The transimpedance operation has been guaranteed
 561 just using a $1M\Omega$ resistor. Other information about the receiver and the transmitter are resumed
 562 in Table II. The experimental validation concerned 16-PPM/2-FSK/4-PAM with $\beta=0.05$, chosen
 563 since representing the most efficient scheme in terms of spectral efficiency and reliability among
 564 those ones previously investigated.

565 In detail, we evaluated the communication performance by transmitting a sequence of 10^8
 566 symbols over two different link distances, that are 175 cm and 75 cm, where we measured a
 567 SNR equal to 5.6 dB and 13.9 dB, respectively. Regarding signal detection, we implemented
 568 the optimum receiver and the QOR, with this latter demonstrating to be the most effective sub-
 569 optimal detector. The results, expressed in terms of BER, are reported in Table III. For the two
 570 considered receivers and communication distances, we compared the BER values achieved with
 571 simulations and experiments. Specifically, it is possible to appreciate that test results only slightly

572 differ from those ones related to simulations. The really limited mismatch is due to the fact that
573 the realized test-bed is not a pure single LED-single PD point-to-point link, so the propagation
574 suffers from different angular emissions paths that are not accounted in the simulation model.
575 However, it is possible to appreciate that at 75cm we achieve a BER of $3.3 \cdot 10^{-7}$ where the
576 simulations report $2 \cdot 10^{-7}$. Obviously, at 175cm the BER is higher for both the cases (simulated
577 and experiments) since the SNR is really low.

578 V. CONCLUSION

579 In this work we have proposed a novel joint modulation approach, based on different tech-
580 niques, namely PAM, FSK and PPM. The main idea is to combine the different schemes in order
581 to exploit their key features and limit the disadvantages of each modulation. The selection of the
582 different schemes is based on the rationale that we can exploit in an effective way amplitude,
583 frequency and time information. The combination of the different schemes is not trivial, and they
584 have to be combined in order to keep a constant power level in a VLC system that is thought for
585 illumination and communication simultaneously. In particular, we have proposed a framework
586 that has been proven, both with a numerical evaluation and experimental results, to be effective
587 and outperform block coding schemes. The proof of concept demonstrates the feasibility of the
588 system, by the means of commercial components, such as LED and PDs, that do not require
589 complex, ad-hoc hardware to integrate the framework. Performance results are very encouraging
590 and prove not only the feasibility of such a kind of frameworks, but also the superiority in
591 respect of block coding based approaches.

592 ACKNOWLEDGMENT

593 This publication has been based upon work from COST Action CA19111 NEWFOCUS,
594 supported by COST (European Cooperation in Science and Technology).

595 REFERENCES

- 596 [1] D. J. Langley, J. van Doorn, I. C. Ng, S. Stieglitz, A. Lazovik, and A. Boonstra, "The internet of everything: Smart
597 things and their impact on business models," *Journal of Business Research*, vol. 122, pp. 853–863, 2021. [Online].
598 Available: <https://www.sciencedirect.com/science/article/pii/S014829631930801X>
- 599 [2] Z. Ghassemlooy, S. Arnon, M. Uysal, Z. Xu, and J. Cheng, "Emerging optical wireless communications-advances and
600 challenges," *IEEE Journal on Selected Areas in Communications*, vol. 33, no. 9, pp. 1738–1749, 2015.
- 601 [3] Y. Zhang, L. Wang, K. Wang, K. S. Wong, and K. Wu, "Recent advances in the hardware of visible light communication,"
602 *IEEE Access*, vol. 7, pp. 91 093–91 104, 2019.

- 603 [4] D. Karunatilaka, F. Zafar, V. Kalavally, and R. Parthiban, "LED based indoor visible light communications: State of the
604 art," *IEEE Communications Surveys & Tutorials*, vol. 17, no. 3, pp. 1649–1678, 2015.
- 605 [5] S. Doğan Tusha, A. Tusha, E. Basar, and H. Arslan, "Multidimensional index modulation for 5G and beyond wireless
606 networks," *Proceedings of the IEEE*, vol. 109, no. 2, pp. 170–199, 2021.
- 607 [6] H. A. Ngo, C. Xu, S. Sugiura, and L. Hanzo, "Space-time-frequency shift keying for dispersive channels," *IEEE Signal
608 Processing Letters*, vol. 18, no. 3, pp. 177–180, 2011.
- 609 [7] G. M. Yamga, A. R. Ndjiongue, and K. Ouahada, "Low complexity clipped frequency shift keying (FSK) for visible light
610 communications," in *2018 IEEE 7th International Conference on Adaptive Science Technology (ICAST)*, 2018, pp. 1–6.
- 611 [8] R. Lee, K. Yun, J.-H. Yoo, S.-Y. Jung, and J. K. Kwon, "Performance analysis of M-ary PPM in dimmable visible light
612 communications," in *2013 Fifth International Conference on Ubiquitous and Future Networks (ICUFN)*, 2013, pp. 380–383.
- 613 [9] S. Arnon, "The effect of clock jitter in visible light communication applications," *J. Lightwave Technol.*, vol. 30, no. 21,
614 pp. 3434–3439, Nov 2012. [Online]. Available: <http://opg.optica.org/jlt/abstract.cfm?URI=jlt-30-21-3434>
- 615 [10] H. G. Batshon and I. B. Djordjevic, "Beyond 240 gb/s per wavelength optical transmission using coded hybrid
616 subcarrier/amplitude/phase/polarization modulation," *IEEE Photonics Technology Letters*, vol. 22, no. 5, pp. 299–301,
617 2010.
- 618 [11] X. Liu, S. Chandrasekhar, T. H. Wood, R. W. Tkach, P. J. Winzer, E. C. Burrows, and A. R. Chraplyvy,
619 "M-ary pulse-position modulation and frequency-shift keying with additional polarization/phase modulation for
620 high-sensitivity optical transmission," *Opt. Express*, vol. 19, no. 26, pp. B868–B881, Dec 2011. [Online]. Available:
621 <http://opg.optica.org/oe/abstract.cfm?URI=oe-19-26-B868>
- 622 [12] A. W. Azim, Y. Le Guennec, and L. Ros, "Hybrid Frequency and Phase-Shift Keying Modulation for Energy
623 Efficient Optical Wireless Systems," *IEEE Wireless Communications Letters*, pp. 1–4, Nov. 2019. [Online]. Available:
624 <https://hal.archives-ouvertes.fr/hal-02383633>
- 625 [13] M. A. Atta and A. Bermak, "A 160 m visible light communication link using hybrid undersampled phase-frequency shift
626 on-off keying and CMOS image sensor," *Opt. Express*, vol. 27, no. 3, pp. 2478–2487, Feb 2019. [Online]. Available:
627 <http://opg.optica.org/oe/abstract.cfm?URI=oe-27-3-2478>
- 628 [14] H. S. Khallaf, H. M. H. Shalaby, J. M. Garrido-Balsells, and S. Sampei, "Performance analysis of a hybrid QAM-MPPM
629 technique over turbulence-free and gamma-gamma free-space optical channels," *Journal of Optical Communications and
630 Networking*, vol. 9, no. 2, pp. 161–171, 2017.
- 631 [15] Y. Xu, Z. Chen, Z. Gong, Z. Xia, T. Yuan, Z. Gu, W. Zhao, and J. Chen, "Hybrid modulation scheme for visible
632 light communication using CMOS camera," *Optics Communications*, vol. 440, pp. 89–94, 2019. [Online]. Available:
633 <https://www.sciencedirect.com/science/article/pii/S0030401819300550>
- 634 [16] Z. Hua, T. Lu, Y. Huang, J. Zhang, S. Dang, and W. Zhao, "Three-dimensional constellation modulated visible light
635 communications with pixelated addressable micro-LED array," in *2019 IEEE 2nd International Conference on Electronics
636 and Communication Engineering (ICECE)*, 2019, pp. 172–177.
- 637 [17] T.-C. Bui, R. Singh, T. O'Farrell, and M. Biagi, "Energy-constrained slot-amplitude modulation with dimming support,"
638 *IEEE Photonics Technology Letters*, vol. 30, no. 14, pp. 1301–1304, 2018.
- 639 [18] —, "Optical energy-constrained slot-amplitude modulation for dimmable vlc: Suboptimal detection and performance
640 evaluation," *IEEE Transactions on Wireless Communications*, vol. 20, no. 3, pp. 1582–1595, 2021.
- 641 [19] J. G. Proakis and M. Salehi, *Digital Communications*, 5th ed. McGraw-Hill, 2008.
- 642 [20] A. Petroni, G. Scarano, R. Cusani, and M. Biagi, "Modulation precoding for MISO visible light communications," *Journal
643 of Lightwave Technology*, vol. 39, no. 17, pp. 5439–5448, 2021.

- 644 [21] J. Ma, J. He, J. Shi, J. He, Z. Zhou, and R. Deng, "Nonlinear compensation based on K-means clustering algorithm for
645 nyquist PAM-4 VLC system," *IEEE Photonics Technology Letters*, vol. 31, no. 12, pp. 935–938, 2019.
- 646 [22] L. Wang, X. Wang, J. Kang, and C. P. Yue, "A 75-mb/s RGB PAM-4 visible light communication transceiver system with
647 pre- and post-equalization," *Journal of Lightwave Technology*, vol. 39, no. 5, pp. 1381–1390, 2021.